Journal of Solid State Chemistry 181 (2008) 2559–2564

Contents lists available at ScienceDirect

Journal of Solid State Chemistry

journal homepage: www.elsevier.com/locate/jssc

# Preparation, crystal structure, and photoluminescence of $Ca_2SnO_4$:$Eu^{3+}$, $Y^{3+}$

Hisanori Yamane *, Yusuke Kaminaga, Shunsuke Abe, Takahiro Yamada

*Institute of Multidisciplinary Research for Advanced Materials, Tohoku University, 2-1-1 Katahira, Aoba-ku, Sendai 980-8577, Japan*

ARTICLE INFO

*Article history:*
Received 7 May 2008
Received in revised form
6 June 2008
Accepted 14 June 2008
Available online 19 June 2008

*Keywords:*
$Eu^{3+}$
Calcium tin oxide
Photoluminescence
Powder X-ray diffraction
Rietveld analysis

ABSTRACT

$Eu^{3+}$-doped $Ca_2SnO_4$ (solid solutions of $Ca_{2-x}Eu_{2x}Sn_{1-x}O_4$, $0 \leqslant x \leqslant 0.3$) and $Eu^{3+}$ and $Y^{3+}$-codoped $Ca_2SnO_4$ ($Ca_{1.8}Y_{0.2}Eu_{0.2}Sn_{0.8}O_4$) were prepared by solid-state reaction at 1400 °C in air. Rietveld analysis of the X-ray powder diffraction patterns revealed that $Eu^{3+}$ replaced $Ca^{2+}$ and $Sn^{4+}$ in $Eu^{3+}$-doped $Ca_2SnO_4$, and that $Eu^{3+}$ replaced $Ca^{2+}$ and $Y^{3+}$ replaced $Sn^{4+}$ in $Ca_{1.8}Y_{0.2}Eu_{0.2}Sn_{0.8}O_4$. Red luminescence at 616 nm due to the electric dipole transition $^5D_0 \rightarrow {}^7F_2$ was observed in the photoluminescence (PL) spectra of $Ca_{2-x}Eu_{2x}Sn_{1-x}O_4$ and $Ca_{1.8}Y_{0.2}Eu_{0.2}Sn_{0.8}O_4$ at room temperature. The maximum PL intensity in the solid solutions of $Ca_{2-x}Eu_{2x}Sn_{1-x}O_4$ was obtained for $x = 0.1$. The PL intensity of $Ca_{1.8}Y_{0.2}Eu_{0.2}Sn_{0.8}O_4$ was 1.26 times greater than that of $Ca_{2-x}Eu_{2x}Sn_{1-x}O_4$ with $x = 0.1$.



## 1. Introduction

Recently, studies on alkaline-earth stanates for the phosphor host materials of rare-earth activators have been proceeding and photoluminescence (PL) properties have been reported for $CaSnO_3$:$Eu^{3+}$, $Pr^{3+}$, $Tb^{3+}$ [1–3], $SrSnO_3$:$Eu^{3+}$, $Tb^{3+}$–$Mg^{2+}$ [1,4], $Ca_2SnO_4$:$Eu^{3+}$ [5,6], $Sr_2SnO_4$:$Eu^{3+}$, $Eu^{3+}$–$Ti^{4+}$ [4,7,8], and $Ba_2SnO_4$:$Eu^{3+}$ [9]. Chen et al. [5] synthesized $(Ca_{1-x}Eu_x)_2SnO_4$ solid solutions at 1100–1300 °C by solid-state reaction and showed the solution limit of Eu($x$) at 0.07 by X-ray powder diffraction. They speculated that some defects introduced by the substitution of $Eu^{3+}$ for $Ca^{2+}$ increased the lattice parameters of the solid solutions. Yang et al. [6] prepared a sample with a composition of $(Ca_{0.95}Eu_{0.05})_2SnO_4$ at 1250 °C by solid-state reaction. Although the obtained sample was mostly Eu-doped $Ca_2SnO_4$ it contained a small amount of $CaSnO_3$. The lattice parameters of the Eu-doped $Ca_2SnO_4$ were larger than those of $Ca_2SnO_4$ [10], although the ionic radius of $Eu^{3+}$ is smaller than that of $Ca^{2+}$ [11]. They considered the increase of the lattice parameters to be due to the effect of the coordination number on the radius of the ions with unsaturated electron configuration. Both papers on Eu-doped $Ca_2SnO_4$ reported an intense peak by the $f$–$f$ transition of $Eu^{3+}$ at around 615–618 nm in the PL spectra and a broad peak due to the charge transfer state (CTS) in the PL excitation spectra.

In a previous study by the present authors, solid solutions of $Ca_{2-x}Y_{2x}Sn_{1-x}O_4$ ($0 < x < 0.5$) were prepared at 1400 °C by solid-state reaction in the system of Ca–Y–Sn–O [12]. The compositions of the single-phase formation and the relationship between the compositions and lattice parameters of $Ca_{2-x}Y_{2x}Sn_{1-x}O_4$ indicated that equi-molar $Ca^{2+}$ and $Sn^{4+}$ ions were replaced by $Y^{3+}$ ions. In the present study, we focused on the preparation and lattice parameters of $Ca_{2-x}Eu_{2x}Sn_{1-x}O_4$ solid solutions. The distribution of $Eu^{3+}$ in the structures was investigated by the Rietveld method for X-ray powder diffraction. The luminescence properties of the solid solutions were compared with those of $Eu^{3+}$ and $Y^{3+}$-codoped $Ca_2SnO_4$.

## 2. Experimental procedure

$Y_2O_3$ powder (99.99% purity; Rare Metallic) and $SnO_2$ powder (99.9% purity; Sigma-Aldrich) were heated at 1000 °C for 6 h before weighing. $CaCO_3$ powder (99.99% purity; Rare Metallic) was dried at 200 °C. The powders were weighed and mixed in an agate mortar with a pestle. The mixture was pressed into pellets, which were placed on a platinum plate and then heated at 1400 °C for 12 h in an electric furnace. After heating, the samples were cooled to room temperature in the furnace by shutting off the electric power. The obtained pellet samples were powdered in the agate mortar and characterized by powder X-ray diffraction (XRD) using Cu$K\alpha$ radiation with a pyrolitic graphite monochromator, a scintillation counter, and a diffractometer (Rigaku RINT, 40 kV, 40 mA). Powdering, pellet forming, and heating at the same condition were repeated until the XRD pattern did not change. Generally, this process was repeated two or three times. Rietveld analysis of the powder XRD pattern measured with a step width of

* Corresponding author. Fax: +81 22 217 5813.
*E-mail addresses:* yamane@tagen.tohoku.ac.jp (H. Yamane), yamataka@tagen.tohoku.ac.jp (T. Yamada).

0022-4596/$ - see front matter © 2008 Elsevier Inc. All rights reserved.
doi:10.1016/j.jssc.2008.06.033

0.02° was carried out with the computer program RIETAN-2000 [13]. The excitation and emission spectra were recorded at room temperature on a fluorescence spectrophotometer (Hitachi F-4500) equipped with a 150 W xenon lamp as the excitation source.

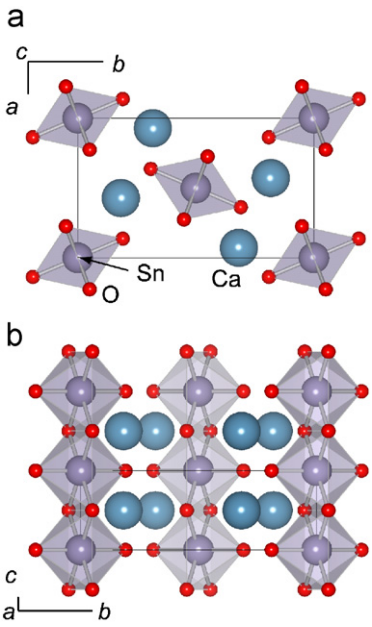


**Fig. 1.** The crystal structure of $Ca_2SnO_4$ projected on the *a*–*b* plane (a) and *b*–*c* plane (b).

## 3. Results and discussion

Samples of $Ca_{2-x}Eu_{2x}Sn_{1-x}O_4$ ($x = 0.0$, 0.001, 0.05, 0.1, 0.15, 0.2, 0.25, 0.3, and 0.4) were prepared at 1400 °C. All peaks in the XRD patterns of the samples prepared with $x = 0.0$–0.3 were indexed with orthorhombic cell parameters (space group *Pbam*). Peaks of CaO and $Eu_2O_3$ appeared in the XRD pattern of the sample prepared with $x = 0.4$. In the structure model of $Ca_2SnO_4$ analyzed by Trömel [10], the Ca atom is at the 4*h* site ($x,y,\frac{1}{2}$) and coordinated by seven oxygen atoms. The Sn atom of the 2*a* site (0,0,0) is coordinated by six oxygen atoms. There are two oxygen sites, the 4*h* site ($x,y,\frac{1}{2}$) and the 4*g* site ($x,y,0$), in the structure. The projections of the crystal structure on the *a*–*b* and *b*–*c* planes are illustrated in Fig. 1 by using the program VESTA [14].

Only the substitution of Eu for Ca was considered in the previous studies on $Ca_2SnO_4$:$Eu^{3+}$ phosphor [5,6]. On the other hand, the substitution of Eu for Sn with a composition of $Ba_2Sn_{0.925}Eu_{0.075}O_4$ has been reported for $Ba_2SnO_4$:$Eu^{3+}$ phosphor [9]. In the present study, we analyzed the crystal structure of $Ca_{2-x}Eu_{2x}Sn_{1-x}O_4$ by Rietveld analysis of X-ray powder diffraction with the model of Eu substitution for Ca and Sn in the structure of $Ca_2SnO_4$. Table 1 summarizes the results of structure refinement for the samples with $x = 0.0$, 0.1, and 0.3. Fig. 2(a) shows the observed and calculated XRD pattern of $Ca_{2-x}Eu_{2x}Sn_{1-x}O_4$ ($x = 0.3$), as an example. Conventional agreement factors for the

**Table 1**
Crystallographic data and structure refinement for $Ca_{2-x}Eu_{2x}Sn_{1-x}O_4$ ($x = 0.0$, 0.1, 0.3) and $Ca_{1.8}Y_{0.2}Eu_{0.2}Sn_{0.8}O_4$

| Formula | | | $Ca_2SnO_4$ ($x = 0.0$) | $Ca_{1.9}Eu_{0.2}Sn_{0.9}O_4$ ($x = 0.1$) | $Ca_{1.7}Eu_{0.6}Sn_{0.7}O_4$ ($x = 0.3$) | $Ca_{1.8}Y_{0.2}Eu_{0.2}Sn_{0.8}O_4$ |
|---|---|---|---|---|---|---|
| Unit cell dimensions | | | | | | |
| | | *a* (Å) | 5.75379(14) | 5.76322(8) | 5.78238(17) | 5.76582(7) |
| | | *b* (Å) | 9.7016(3) | 9.7997(13) | 9.7868(3) | 9.76949(11) |
| | | *c* (Å) | 3.26641(8) | 3.28937(4) | 3.33566(9) | 3.30489(4) |
| Cell volume | | *V* (Å$^3$) | 182.334(8) | 184.644(4) | 188.767(9) | 186.162(4) |
| *Z* | | | 2 | 2 | 2 | 2 |
| Goodness-of-fit | | | 2.462 | 1.413 | 1.326 | 1.382 |
| *R* value | | $R_{wp}$ (%) | 10.98 | 9.25 | 10.40 | 9.20 |
| | | $R_p$ (%) | 7.88 | 6.75 | 7.60 | 6.67 |
| | | $R_I$ (%) | 4.68 | 1.66 | 2.89 | 1.98 |
| | | $R_F$ (%) | 2.45 | 1.05 | 1.66 | 1.08 |
| Atom Site | | | | | | |
| Ca/Eu | 4*h* | *g* | 1.00/0.00 | 0.95(1)/0.05 | 0.85(1)/0.15 | 0.90/0.10 |
| | | *x* | 0.0718(2) | 0.06870(16) | 0.0661(2) | 0.06896(15) |
| | | *y* | 0.31768(13) | 0.31820(11) | 0.32111(15) | 0.31906(10) |
| | | *z* | 0.5 | 0.5 | 0.5 | 0.5 |
| | | *B* (Å$^2$) | 0.87(3) | 0.276(16) | 0.41(3) | 0.40(2) |
| Sn/Y/Eu | 2*a* | *g* | 1.00/0.00/0.00 | 0.90(6)/0.00/0.10 | 0.70(10)/0.00/0.30 | 0.60/0.20/0.00 |
| | | x | 0 | 0 | 0 | 0 |
| | | *y* | 0 | 0 | 0 | 0 |
| | | *z* | 0 | 0 | 0 | 0 |
| | | *B* (Å$^2$) | 0.620(14) | 0.276[a] | 0.41[a] | 0.199(12) |
| O1 | 4*h* | *g* | 1.0 | 1.0 | 1.0 | 1.0 |
| | | *x* | 0.2257(6) | 0.2312(6) | 0.2443(10) | 0.2289(6) |
| | | *y* | 0.0502(4) | 0.0491(3) | 0.0491(6) | 0.0482(4) |
| | | *z* | 0.5 | 0.5 | 0.5 | 0.5 |
| | | *B* (Å$^2$) | 0.47(6) | 0.27(8) | 0.74(13) | 0.66(6) |
| O2 | 4*g* | *g* | 1.0 | 1.0 | 1.0 | 1.0 |
| | | *x* | 0.3631(6) | 0.3613(6) | 0.3565(9) | 0.3601(6) |
| | | *y* | 0.3097(4) | 0.3061(4) | 0.3049(6) | 0.3063(4) |
| | | *z* | 0 | 0 | 0 | 0 |
| | | *B* (Å$^2$) | 0.47[b] | 0.27[b] | 0.74[b] | 0.66 |

[a] Constrained with the value of Ca/Eu.
[b] Constrained with the value of O1.

Rietveld analysis for the sample of $x = 0.3$ resulted in $R_{wp} = 10.40\%$, $R_I = 2.89\%$, $R_F = 1.66\%$, and goodness-of-fit $S = 1.326$.

The refined cell parameters and cell volume of $Ca_{2-x}Eu_{2x}Sn_{1-x}O_4$ against the Eu content $x$ are plotted in Fig. 3. The cell parameters of $Ca_2SnO_4$ ($a = 5.7586(1)$, $b = 9.7097(1)$, and $c = 3.2692$ (1) Å) agreed with those reported by Trömel ($a = 5.748(1)$, $b = 9.694(1)$, and $c = 3.264(1)$ Å) [10]. The $a$- and $c$-axis lengths increased linearly in the range $x = 0$–0.3, where the single phases of $Ca_{2-x}Eu_{2x}Sn_{1-x}O_4$ were obtained. The $b$-axis length also monotonically increased in this range of $x$.

Table 2 summarizes the metal–oxygen interatomic distances calculated with the refined parameters for $Ca_{2-x}Eu_{2x}Sn_{1-x}O_4$ ($x = 0.0$, 0.1, 0.3). All interatomic distances between the Sn/Eu site and the oxygen sites increased with $x$. The average of the Sn/Eu–O distances for $x = 0.1$ and 0.3 was, respectively, 1.5% and 4.2% larger than that of the Sn–O distances in $Ca_2SnO_4$, which corresponded to a 5.0% and a 13.6% increase of the volume of Sn/Eu centered oxygen octahedron (Sn/Eu–$O_6$), respectively. These relations are consistent with the relation of the effective ionic radii ($Sn^{4+}$, 0.690 Å and $Eu^{3+}$, 0.947 Å) proposed by Shannon [11]. Since the ionic radii of $Ca^{2+}$ and $Eu^{3+}$ in sevenfold coordination are 1.06 and 1.01 Å, respectively, it was expected that all Ca/Eu–O distances would decrease as a result of the $Eu^{3+}$ substitution. However, some of the distances increased, probably, due to the increase of the Sn/Eu–O distances or the volume increase of the Sn/Eu–$O_6$ octahedron. The average of the Ca/Eu–O interatomic distances slightly increased from 2.440 Å ($x = 0$) to 2.449 Å ($x = 0.3$). As shown in Fig. 4, the cell parameters of the sample with $x = 0.3$ are 0.50% and 0.88% larger for the $a$- and $b$-axes and 2.12% for the $c$-axis. The larger increase of the $c$-axis length directly reflected the volume increase of the Sn/Eu–$O_6$ octahedra, which extend along the $c$-axis by sharing the edges (see Fig. 1(b)).

In the previous study reported by Yang et al. [6], a single-phase solid solution was not obtained and $CaSnO_3$ was included in the sample prepared with a composition of $x = 0.05$ for $(Ca_{1-x}Eu_x)_2SnO_4$. Our results indicated that this finding was obtained because only the substitution of Eu for Ca was considered. The Eu substitution range of $x = 0.3$ for $Ca_{2-x}Eu_{2x}Sn_{1-x}O_4$ was wider than $x \leqslant 0.07$ of $(Ca_{1-x}Eu_x)_2SnO_4$ reported by Chen et al. [5]. Also, the increase of the lattice parameters observed in the previous studies was caused neither by defects nor by unsaturated electron configuration, but rather by the substitution of Eu for Sn at the octahedral site.

We prepared $Ca_{1.8}Y_{0.2}Eu_{0.2}Sn_{0.8}O_4$ containing the same amount of Eu as that in the formula of $Ca_{1.9}Eu_{0.2}Sn_{0.9}O_4$, which showed the highest intensity among the solid solutions $Ca_{2-x}Eu_{2x}Sn_{1-x}O_4$, as mentioned in the following section. The powder XRD pattern of $Ca_{1.8}Y_{0.2}Eu_{0.2}Sn_{0.8}O_4$ is shown in Fig. 2(b). In order to clarify the site occupancies of Eu and Y, Rietveld analysis was performed with the models shown in Table 3. In model A, only $Eu^{3+}$ ions occupy the Ca site ($4h$) and only $Y^{3+}$ ions occupy the Sn site ($2a$). Both Ca and Sn sites are occupied by the same amount (0.100) of Eu and Y in model C. Model E shows the occupation of the Sn site by $Eu^{3+}$ ions and that of the Ca site by $Y^{3+}$ ions. Agreement factors of the analyses are also summarized in Table 3. The best fit between the observed and calculated XRD patterns was obtained by model A with the lowest agreement factors, e.g., $R_{wp} = 9.20$ and $S = 1.382$. Table 1 shows the refined lattice parameters, atomic coordinates, and isotropic displacement parameters of $Ca_{1.9}Eu_{0.2}Sn_{0.9}O_4$. The ionic radius of $Y^{3+}$ in sixfold coordination

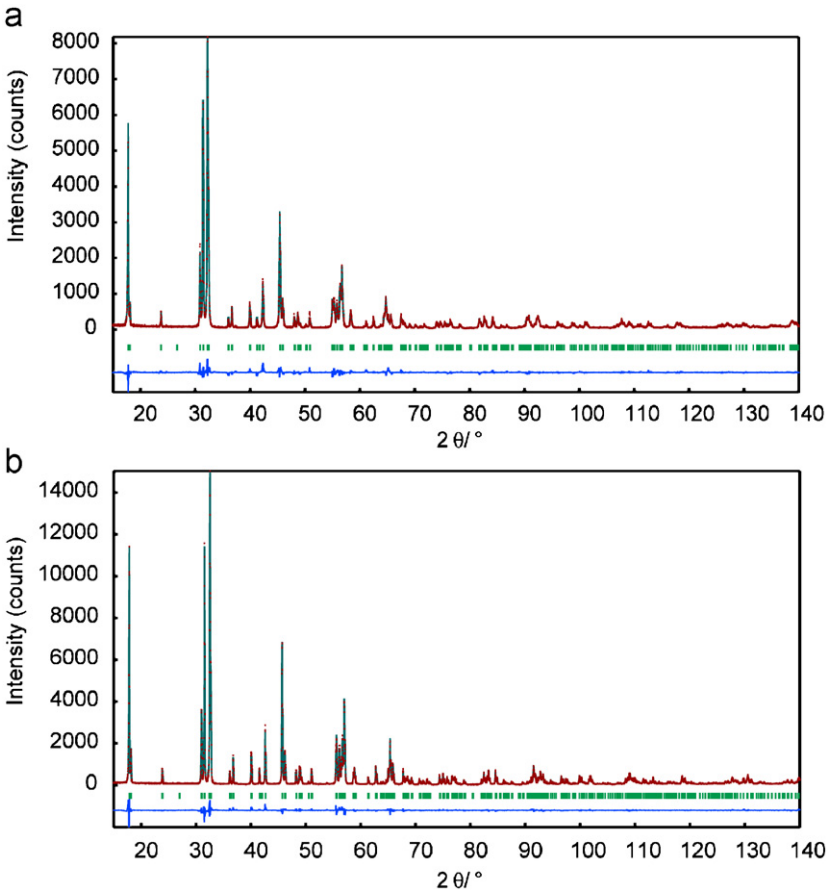


**Fig. 2.** The observed (dots) and calculated (solid) X-ray diffraction profiles of $Ca_{1.7}Eu_{0.6}Sn_{0.7}O_4$ (a) and $Ca_{1.8}Y_{0.2}Eu_{0.2}Sn_{0.8}O_4$ (b). The short vertical bars show the positions of the allowed Bragg reflections. The difference profile is located at the bottom of the figures.

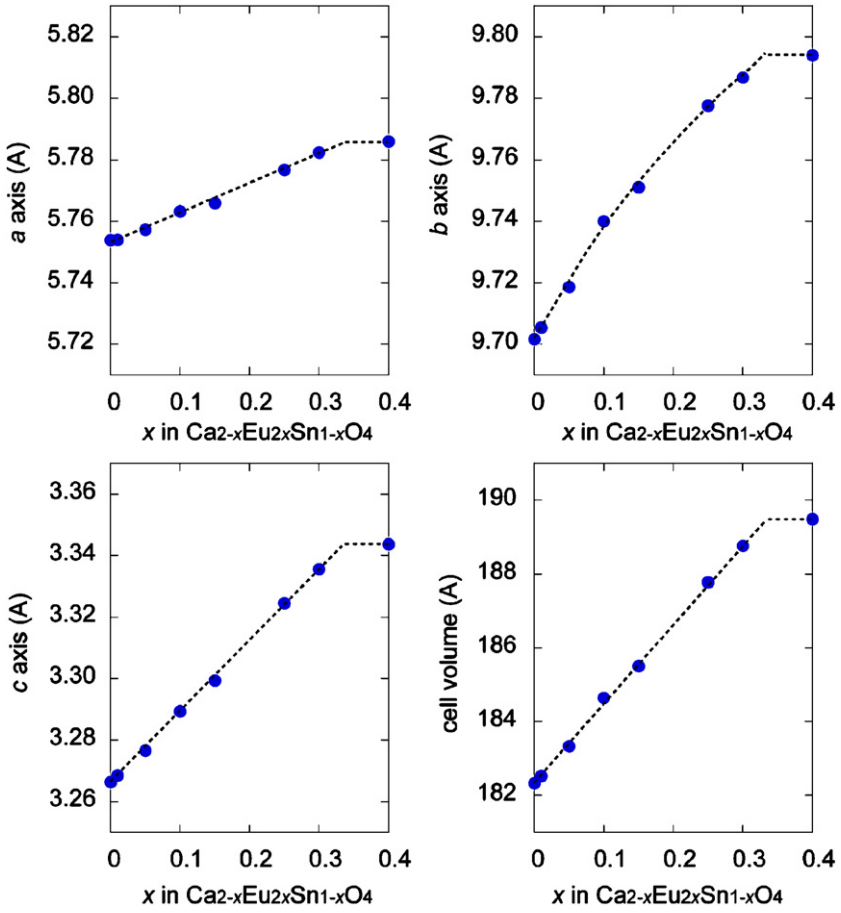


**Fig. 3.** Cell parameters and volume versus $Eu^{3+}$ content $x$ in $Ca_{2-x}Eu_{2x}Sn_{1-x}O_4$. Estimated standard deviations are within the plotted marks.

**Table 2**
Selected interatomic distances (Å) of $Ca_{2-x}Eu_{2x}Sn_{1-x}O_4$ ($x = 0.0$, 0.1, 0.3) and $Ca_{1.8}Y_{0.2}Eu_{0.2}Sn_{0.8}O_4$

| | $Ca_2SnO_4$ ($x = 0.0$) | $Ca_{1.9}Eu_{0.2}Sn_{0.9}O_4$ ($x = 0.1$) | $Ca_{1.7}Eu_{0.6}Sn_{0.7}O_4$ ($x = 0.3$) | $Ca_{1.8}Y_{0.2}Eu_{0.2}Sn_{0.8}O_4$ |
|---|---|---|---|---|
| Ca/Eu—O2 | 2.342(3) × 2 | 2.359(3) × 2 | 2.372(4) × 2 | 2.359(2) × 2 |
| Ca/Eu—O1 | 2.368(4) | 2.3351(4) | 2.253(6) | 2.351(3) |
| Ca/Eu—O2 | 2.374(3) × 2 | 2.366(3) × 2 | 2.403(4) × 2 | 2.384(3) × 2 |
| Ca/Eu—O1 | 2.539(4) | 2.527(4) | 2.486(6) | 2.523(4) |
| Ca/Eu—O1 | 2.742(4) | 2.783(4) | 2.855(6) | 2.803(4) |
| Average (Å) | 2.440 | 2.442 | 2.449 | 2.452 |
| Volume (Å$^3$) | 20.05 | 20.12 | 20.34 | 20.36 |
| Sn/Y/Eu—O2 | 2.008(4) × 2 | 2.051(3) × 2 | 2.082(6) × 2 | 2.057(4) × 2 |
| Sn/Y/Eu—O1 | 2.143(2) × 4 | 2.170(2) × 4 | 2.238(4) × 4 | 2.166(2) × 4 |
| Average (Å) | 2.098 | 2.130 | 2.186 | 2.130 |
| Volume (Å$^3$) | 12.115 | 12.716 | 13.768 | 12.674 |

(0.90 Å) is closer to that of $Sn^{4+}$ (0.690 Å) than the radius of $Eu^{3+}$ (0.947 Å), while the ionic radii of $Ca^{2+}$ and $Eu^{3+}$ (1.06 and 1.01 Å, respectively) are larger than the radius of $Y^{3+}$ in sevenfold coordination (0.96 Å). These size relations correspond to the occupation of the Ca site by $Eu^{3+}$ ions and that of the Sn site by $Y^{3+}$ ions in $Ca_{1.8}Y_{0.2}Eu_{0.2}Sn_{0.8}O_4$.

Fig. 5 shows the PL spectrum of $Ca_{1.9}Eu_{0.2}Sn_{0.9}O_4$ under 288 nm excitation. A strong emission peak due to the electric dipole transition $^5D_0 \rightarrow {}^7F_2$ was observed at 616 nm. The electric dipole transition is induced by the lack of inversion symmetry at the $Eu^{3+}$ site and depends strongly on the site symmetry in a host crystal. In the structure of $Ca_{1.9}Eu_{0.2}Sn_{0.9}O_4$, $Eu^{3+}$ ions occupy both the Ca site (4*h*) and the Sn site (2*a*). The local symmetry of the Sn site is centrosymmetric 2/*m*. The non-centrosymmetric Ca site (*m*) is coordinated by seven oxygen atoms. Thus, the strong emission of the $^5D_0 \rightarrow {}^7F_2$ transition is mainly attributed to the $Eu^{3+}$ ions which occupy the Ca site.

The PL intensity dependence of the Eu content $x$ in $Ca_{2-x}Eu_{2x}Sn_{1-x}O_4$ is shown in Fig. 6. The intensity at 616 nm became higher with $x$ up to 0.1 (10 mol%), which was close to the Eu content (7 mol%) of $Ca_2SnO_4$:$Eu^{3+}$ with the maximum intensity in the study by Chen et al. [5]. The decrease of the intensity at higher Eu contents could probably be explained as being due to cross-relaxation.

The PL spectrum from $Ca_{1.8}Y_{0.2}Eu_{0.2}Sn_{0.8}O_4$, in which the Eu content in the formula was same as that in the formula of $Ca_{1.9}Eu_{0.2}Sn_{0.9}O_4$, is also depicted in Fig. 5. The emission intensity of $Ca_{1.8}Y_{0.2}Eu_{0.2}Sn_{0.8}O_4$ at 616 nm was 1.26 times higher than that

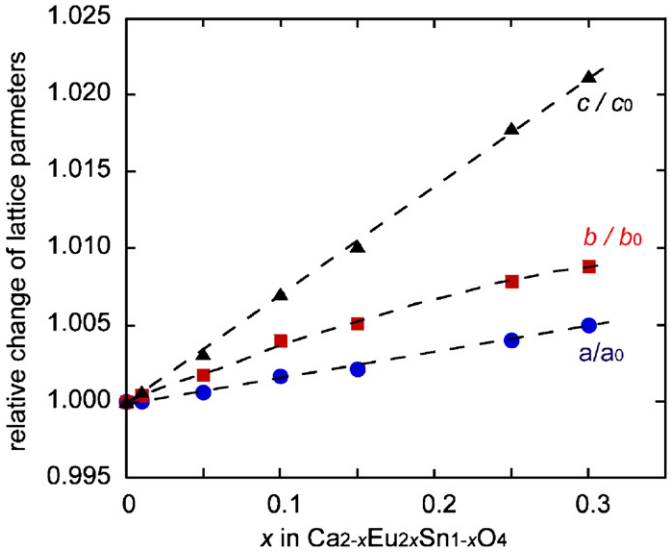


**Fig. 4.** $Eu^{3+}$ content dependence of the cell parameters normalized with the values at $x = 0$.

**Table 3**
Structure refinement for $Ca_{1.8}Y_{0.2}Eu_{0.2}Sn_{0.8}O_4$ with various site occupancies

| Site | | Site occupancy $g$ | | | | |
|---|---|---|---|---|---|---|
| | Model | A | B | C | D | E |
| 4*h* | Ca1 | 0.900 | 0.900 | 0.900 | 0.900 | 0.900 |
| | Y1 | 0.000 | 0.025 | 0.050 | 0.075 | 0.100 |
| | Eu1 | 0.100 | 0.075 | 0.050 | 0.025 | 0.000 |
| 2*a* | Sn2 | 0.800 | 0.800 | 0.800 | 0.800 | 0.800 |
| | Y2 | 0.200 | 0.150 | 0.100 | 0.050 | 0.000 |
| | Eu2 | 0.000 | 0.050 | 0.100 | 0.150 | 0.200 |
| 4*h* | O1 | 1.000 | 1.000 | 1.000 | 1.000 | 1.000 |
| 4*g* | O2 | 1.000 | 1.000 | 1.000 | 1.000 | 1.000 |
| $R_{WP}$ | | 9.20 | 9.37 | 9.73 | 10.36 | 11.26 |
| $R_P$ | | 6.67 | 6.82 | 7.09 | 7.53 | 8.16 |
| $R_I$ | | 1.98 | 1.98 | 2.41 | 3.04 | 4.06 |
| $R_F$ | | 1.08 | 1.06 | 1.16 | 1.35 | 1.65 |
| $S$ | | 1.382 | 1.409 | 1.462 | 1.557 | 1.693 |

of $Ca_{1.9}Eu_{0.2}Sn_{0.9}O_4$. As mentioned above, the structure formula of $Ca_{1.8}Y_{0.2}Eu_{0.2}Sn_{0.8}O_4$ can be expressed with $(Ca_{0.9}Eu_{0.1})_2(Sn_{0.8}Y_{0.2})O_4$, and all $Eu^{3+}$ ions occupy the Ca site. The selective occupation of the nonsymmetric Ca site by $Eu^{3+}$ may have caused the increase of the PL intensity. Separation of $Eu^{3+}$ ions by the $Y^{3+}$ ion-occupied Sn site may also have reduced Eu–Eu energy transfer.

The excitation spectra of $Ca_{1.9}Eu_{0.2}Sn_{0.9}O_4$ and $Ca_{1.8}Y_{0.2}Eu_{0.2}Sn_{0.8}O_4$ monitored at 616 nm are shown in Figs. 7(a) and (b). In addition to intra-4*f*-shell transitions for $Eu^{3+}$ ions, a broad band attributed to the CTS due to europium–oxygen interaction was observed in the spectra. The CTS band of $Ca_{1.9}Eu_{0.2}Sn_{0.9}O_4$ with a peak at 296 nm was broader than that of $Ca_{1.8}Y_{0.2}Eu_{0.2}Sn_{0.8}O_4$ with a peak at 288 nm. This may also be related to the site selectivity of $Eu^{3+}$ ion in $Ca_{1.8}Y_{0.2}Eu_{0.2}Sn_{0.8}O_4$.

## 4. Conclusions

The substitution of $Eu^{3+}$ ions for both $Ca^{2+}$ and $Sn^{4+}$ ions in $Ca_2SnO_4$ was revealed by solid-state reaction synthesis and Rietveld analysis of X-ray powder diffraction. Single-phase solid

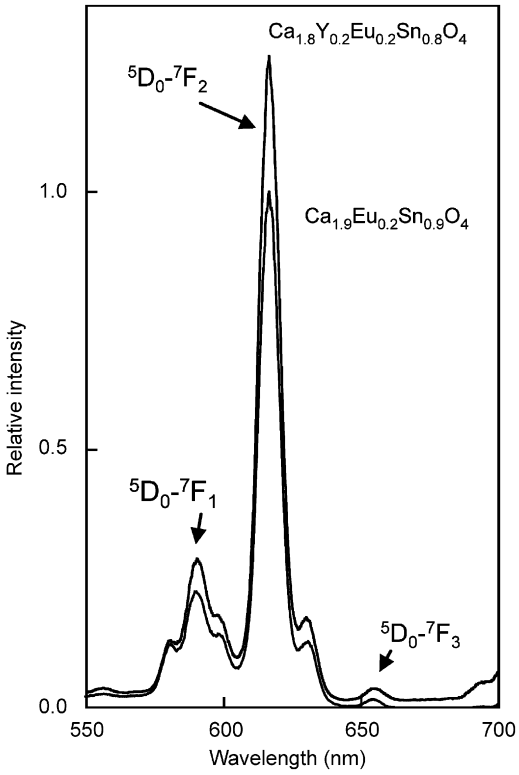


**Fig. 5.** Emission spectra of $Ca_{1.9}Eu_{0.2}Sn_{0.9}O_4$ excited at 296 nm and $Ca_{1.8}Y_{0.2}Eu_{0.2}Sn_{0.8}O_4$ excited at 288 nm.

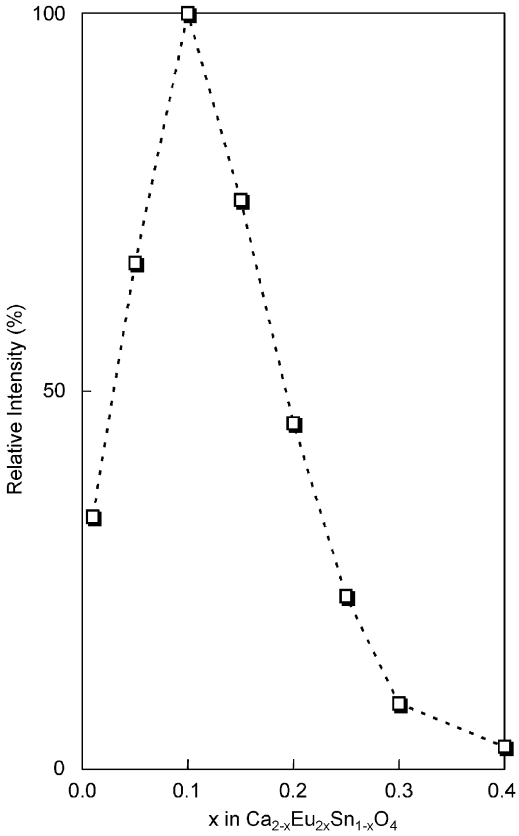


**Fig. 6.** Variation of emission intensity with $Eu^{3+}$ content $x$ in $Ca_{2-x}Eu_{2x}Sn_{1-x}O_4$ (a) under 296 nm excitation.

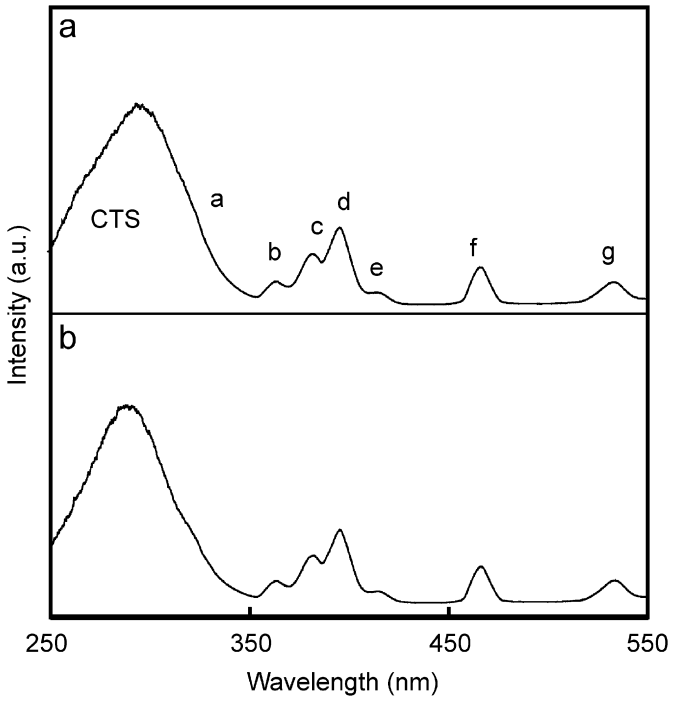


**Fig. 7.** Excitation spectra of $Ca_{1.9}Eu_{0.2}Sn_{0.9}O_4$ (a) and $Ca_{1.8}Y_{0.2}Eu_{0.2}Sn_{0.8}O_4$ (b) monitored at 616 nm.

solutions of $Ca_{2-x}Eu_{2x}Sn_{1-x}O_4$ were prepared at $x \leqslant 0.3$. Selective occupation of the Ca site by $Eu^{3+}$ ions and of the Sn site by $Y^{3+}$ ions was suggested for the sample prepared by co-doping of $Ca_2SnO_4$ with Eu and Y. The highest PL intensity among the solid solutions of $Ca_{2-x}Eu_{2x}Sn_{1-x}O_4$ was observed at 616 nm for the sample with $x = 0.1$ under 296 nm excitation. The intensity of the emission at 616 nm from $Ca_{1.8}Y_{0.2}Eu_{0.2}Sn_{0.8}O_4$ was 1.26 times higher than that from $Ca_{1.9}Eu_{0.2}Sn_{0.9}O_4$.

## Acknowledgments

This work was supported in part by a Science Research Expenses Subsidy from the Ministry of Education, Culture, Sports, Science, and Technology, Japan, Grant-in-Aid for Scientific Research (B), 17360316, 2007.

## References

[1] Z. Lu, L. Chen, Y. Tang, Y. Li, J. Alloys Compd. 387 (2005) L1–L4.
[2] Z. Liu, Y. Liu, Mater. Chem. Phys. 93 (2005) 129–132.
[3] B. Lei, B. Li, H. Zhang, L. Zhang, Y. Cong, W. Li, J. Electrochem. Soc. 154 (2007) H623–H630.
[4] K. Ueda, T. Yamashita, K. Nakayashiki, K. Goto, Jpn. J. Appl. Phys. 45 (2006) 6981–6983.
[5] Y.-C. Chen, Y.-H. Chang, B.-S. Tsai, Opt. Mater. 27 (2005) 1874–1878.
[6] H.M. Yang, J.X. Shi, M.L. Gong, J. Sol. State. Chem. 178 (2005) 917–920.
[7] H.M. Yang, J.X. Shi, M.L. Gong, J. Alloys Compd. 415 (2006) 213–215.
[8] Y.-C. Chen, Y.-H. Chang, B.-S. Tsai, J. Alloys Compd. 398 (2005) 256–260.
[9] H. Gao, Y. Wang, J. Mater. Res. 21 (2006) 1857–1861.
[10] M. Trömel, Z. Anorg. Allg. Chem. 54 (1969) 237–247 (JCPDS ($Ca_2SnO_4$ ≠46-0112).
[11] R.D. Shanon, Acta Crystallogr. A 32 (1976) 751–767.
[12] Y. Kaminaga, H. Yamane, T. Yamada, J. Am. Ceram. Soc. 90 (2007) 1917.
[13] F. Izumi, T. Ikeda, Mater. Sci. Forum 321–324 (2000) 198.
[14] F. Izumi, K. Momma, Solid State Phenom. 130 (2007) 15–20.